Development of inhibitors of SAICAR synthetase (PurC) from *Mycobacterium abscessus* using a fragment-based approach.

Sitthivut Charoensutthivarakul[a,e], Sherine E. Thomas[b], Amy Curran[a], Karen P. Brown[c,d], Juan M. Belardinelli[f], Andrew J. Whitehouse[a], Marta Acebrón-García-de-Eulate[b], Jaspar Sangan[c,d], Subramanian G. Gramani[a], Mary Jackson[f], Vitor Mendes[b], R. Andres Floto[c,d], Tom L. Blundell*[b], Anthony G. Coyne*[a] and Chris Abell[a]

a) Yusuf Hamied Department of Chemistry, University of Cambridge, Lensfield Road, Cambridge, CB2 1EW, UK
b) Department of Biochemistry, University of Cambridge, Tennis Court Road, Cambridge, CB2 1GA, UK.
c) Molecular Immunity Unit, Department of Medicine, MRC Laboratory of Molecular Biology, University of Cambridge, Francis Crick Avenue, Cambridge Biomedical Campus, Cambridge, CB2 0QH, UK
d) Cambridge Centre for Lung Infection, Royal Papworth Hospital, Cambridge, CB23 3RE, UK
e) School of Bioinnovation and Bio-based Product Intelligence, Faculty of Science, Mahidol University, Bangkok, 10400, Thailand
f) Mycobacteria Research Laboratories, Department of Microbiology, Immunology and Pathology, Colorado State University, Fort Collins, Colorado, 80523-1682, USA.

To whom correspondence may be addressed *Anthony Coyne: agc40@cam.ac.uk, * Tom Blundell: tlb20@cam.ac.uk

Abstract

Mycobacterium abscessus (Mab) has emerged as a challenging threat to individuals with cystic fibrosis. Infections caused by this pathogen are often impossible to treat due to the intrinsic antibiotic resistance leading to lung malfunction and eventually death. Therefore, there is an urgent need to develop new drugs against novel targets in *Mab* to overcome drug resistance and subsequent treatment failure. In this study, SAICAR synthetase (PurC) from *Mab* was identified as a promising target for novel antibiotics. An in-house fragment library screen and a high-throughput X-ray crystallographic screen of diverse fragment libraries were explored to provide crucial starting points for fragment elaboration. A series of compounds developed from fragment growing and merging strategies, guided by crystallographic information and careful hit-to-lead optimisation, have achieved potent nanomolar binding affinity against the enzyme. Some compounds also show promising inhibitory effect against *Mab* and *Mtb.* This work utilises a fragment-based design and demonstrates for the first time the potential to develop inhibitors against PurC from *Mab*.

Keywords: structure-guided; fragment-based drug discovery; *Mycobacterium abscessus*; cystic fibrosis; PurC; SAICAR synthetase.

Mycobacterium abscessus (*Mab*) is a rapidly growing species of nontuberculous mycobacteria (NTM) which is responsible for a wide range of soft tissue infections which have emerged as a major threat to individuals with cystic fibrosis.[1-4] These infections and are often impossible to treat due to their intrinsic antibiotic resistance and result in extremely high treatment failure rates of around 55 % despite years of combination chemotherapy and can often prove fatal.[5, 6,7, 8]. The current drug regimen involves a combination of antibiotics, such as Amikacin, and this may take up to two years to be complete. Therefore, there is an urgent need to develop novel drugs targeting *Mab,* as an alternative antibacterial strategy.

Phosphoribosylaminoimidazole succinocarboxamide synthetase or PurC (also known as SAICAR synthetase) is an essential enzyme involved in the *de novo* purine biosynthesis in bacteria and fungi.[9] The enzyme catalyses the transformation of 5-aminoimidazole-4-carboxyribonucleotide (CAIR) and L-aspartate to Phosphoribosylaminoimidazole-succinocarboxamide (SAICAR) in the presence of adenosine triphosphate (ATP) and Mg^{2+} cofactors (Scheme 1).[10, 11]

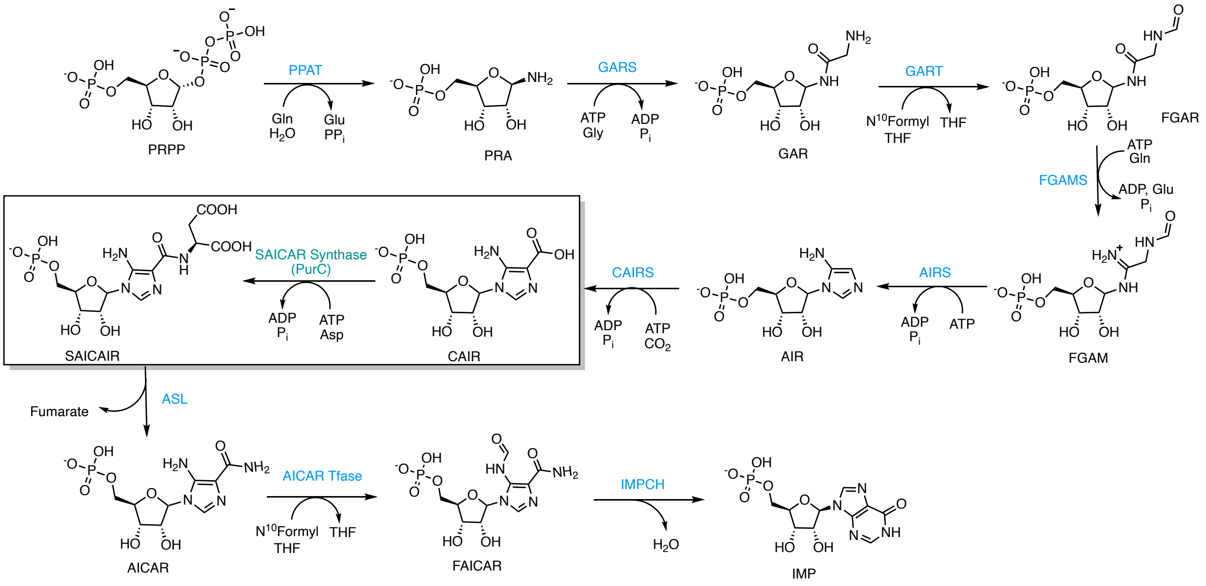

Scheme 1: Purine biosynthetic pathway, the pathway transforms PRPP (phosphoribosyl pyrophosphate) into IMP (inosine monophosphate) in ten biosynthetic steps. SAICAR synthetase (PurC) catalyzes seventh step in the biosynthetic pathway which transforms CAIR (carboxyaminoimidazole ribonucleotide) into SAICAIR (succinylaminoimidazole carboxyamide ribonucleotide) using ATP and L-aspartate.

It is known that bacteria rely on the *de novo* pathway for their survival, as the pathway plays a crucial role in the synthesis of nucleic acid and nucleotide phosphate precursors for energy metabolism. Several studies in the past have shown that purine biosynthesis is vital for bacterial growth and persistence in the gut, blood and lungs.[12-14]

While most bacterial PurC enzymes exist as homo-dimers, *Mab* and *Saccharomyces cerevisiae* orthologs function as monomers.[15-18] In contrast, the human bifunctional ortholog (PAICS) is an octameric enzyme combining a central C-terminal ring of AIR carboxylase domain and an outer N-terminal SAICAR synthetase domain.[19] A comparison of *Mab* PurC and the SAICAR synthetase domain of the human ortholog shows distinct structural and sequence differences, providing the basis for selective inhibition of this enzyme.[20] The structural and functional differences between bacterial PurC and PAICS makes PurC an excellent target for antimicrobial drug discovery.[15, 19, 21, 22]

Fragment-based drug discovery has emerged as a successful approach for the identification of new drugs. Recently, another drug derived from a fragment-based approach secured a breakthrough approval from the FDA and this methodology is seen as a reliable way forward in small-molecule drug design.[23] Fragments are low-molecular-weight molecules with low structural complexity. The hits that come from a fragment-based screening usually exhibit lower potency than larger molecules identified from a standard high-throughput platform. However, these fragments bind by making high-quality interactions to a hotspot on the biomolecular target leading to highly ligand efficient (LE) molecules.[24, 25]

In this work, the application of a fragment-based approach targeting *Mab* SAICAR synthetase (*Mab*PurC) was used to discover a new class of 4-amino-6-(pyrazol-4-yl)pyrimidine based inhibitors. The fragment elaboration strategies described here utilised the hits identified from both our in-house fragment library and XChem fragment screening facilities as starting points for development.[20] Through this study, for the first time, we were able to validate the essentiality of PurC in *Mab* and demonstrate the potential for developing inhibitors against this bacterial enzyme.

RESULTS AND DISCUSSION

Generation of purC gene knock-out mutants

In order to assess the suitability of targeting PurC for anti-microbial drug development, essentiality studies of PurC in *Mab* were performed. This approach made use of a recombineering system to generate knockout mutants in *M. abscessus subsp. massilliense*. The resulting knockouts were analysed by PCR and compared with that of the wild-type. The knockout strains did not grow in normal growth media, but colonies appeared when the media was supplemented with hypoxanthine, thus supporting the essentiality of the *purC* gene in bacterial growth and replication (Figure 1)

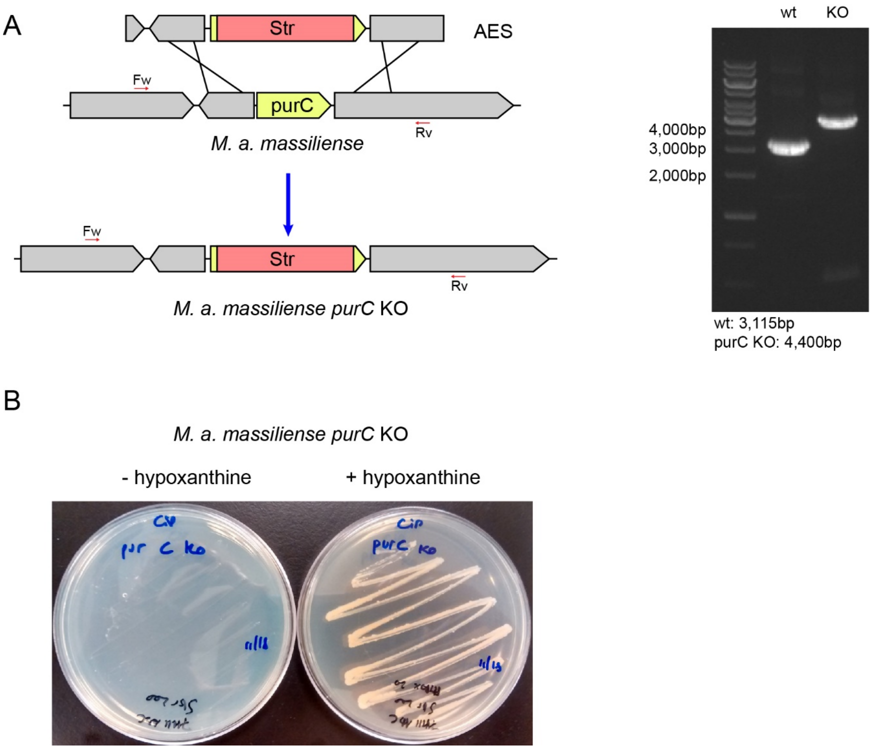

Figure 1: (a). Schematic representation showing recombination of the allelic exchange substrate (AES) into the chromosome of *M. abscessus subsp. massiliense* followed by replacement of *purC* gene with Str cassette and PCR analysis of *M. abscessus subsp. massiliense purC* KO and wt confirming the insertion of the cassette. (b). Essentiality of the *purC* gene: Growth of *M. abscessus subsp. massiliense purC* KO strains on 7H11 ADC plates with or without added hypoxanthine (20 mg/mL)

Initial SAR Studies

Research within our group has identified several fragments that were found to bind into the adenine pocket of the ATP binding site of *M. abscessus* PurC. These were characterised using a range of biophysical techniques, including differential scanning fluorimetry (DSF), isothermal titration calorimetry (ITC) and X-ray crystallography.[20] The fragment hitd were identified using a dual strategy, firstly the screening of an in-house fragment library of 960 fragments and the second was the screening of two diverse fragment libraries (125 and 768 fragments) at the XChem screening platform at the Diamond Light Source. The screening of the in-house fragment library led to the identification of eight fragments which were characterised using a range of biophysical techniques and X-ray crystallography. The screening of the two fragment libraries at XChem led to the identification of thirty five fragments, of which 60% of these were shown to bind at the ATP site by X-ray crystallography. However no biophysical data was available for these fragments. One of the hits identified from the screening of the in-house fragment library was 4-amino-5-pyrimidinecarbonitrile, fragment **1**. The X-ray crystal structure of *Mab*PurC in complex with this fragment shows several key interactions which include i) H-bonding of the amino moiety of **1** to the His69 side chain and to the main chain carbonyl of R91 ii) H-bonding of the N3 of pyrimidine to the amide nitrogen of Leu93 and iii) H-bonding of the nitrile nitrogen to the amide nitrogen of D213. These interactions are also made by the adenine ring of ATP when it binds to PurC. Along with its well-characterised interactions, this fragment also demonstrated a ΔT_m of +3.6^{o}C and a K_d value of 340 μM (for ATP; K_d = 88 μM).

A further fragment screen was also performed on *Mab*PurC with a more structurally diverse library using the high-throughput X-ray screening approach (XChem) available at the Diamond Light Source.[26] With the access to the roboticised XChem facility [27, 28], fragment **2** was identified and its binding interactions to *Mab*PurC were characterised (Figure 2).[20,30,] One of the distinct interactions that this fragment makes is the π-interaction between pyridine ring of the fragment **2** and the side chain of R17. The movement of the Arg side chain to accommodate the pyridine ring of fragment **2** was not previously observed from our in-house fragment screening and is not observed in the ATP-bound structure (PDB Code 6YX3), (Figure 2f**)**. The flexibility of this R17 side chain was identified as beneficial towards further medicinal chemistry intervention to design chemical scaffolds that possess a slightly different mode of binding to that of ATP. This important aspect was therefore incorporated into a fragment-growing strategy from the ATP binding site.

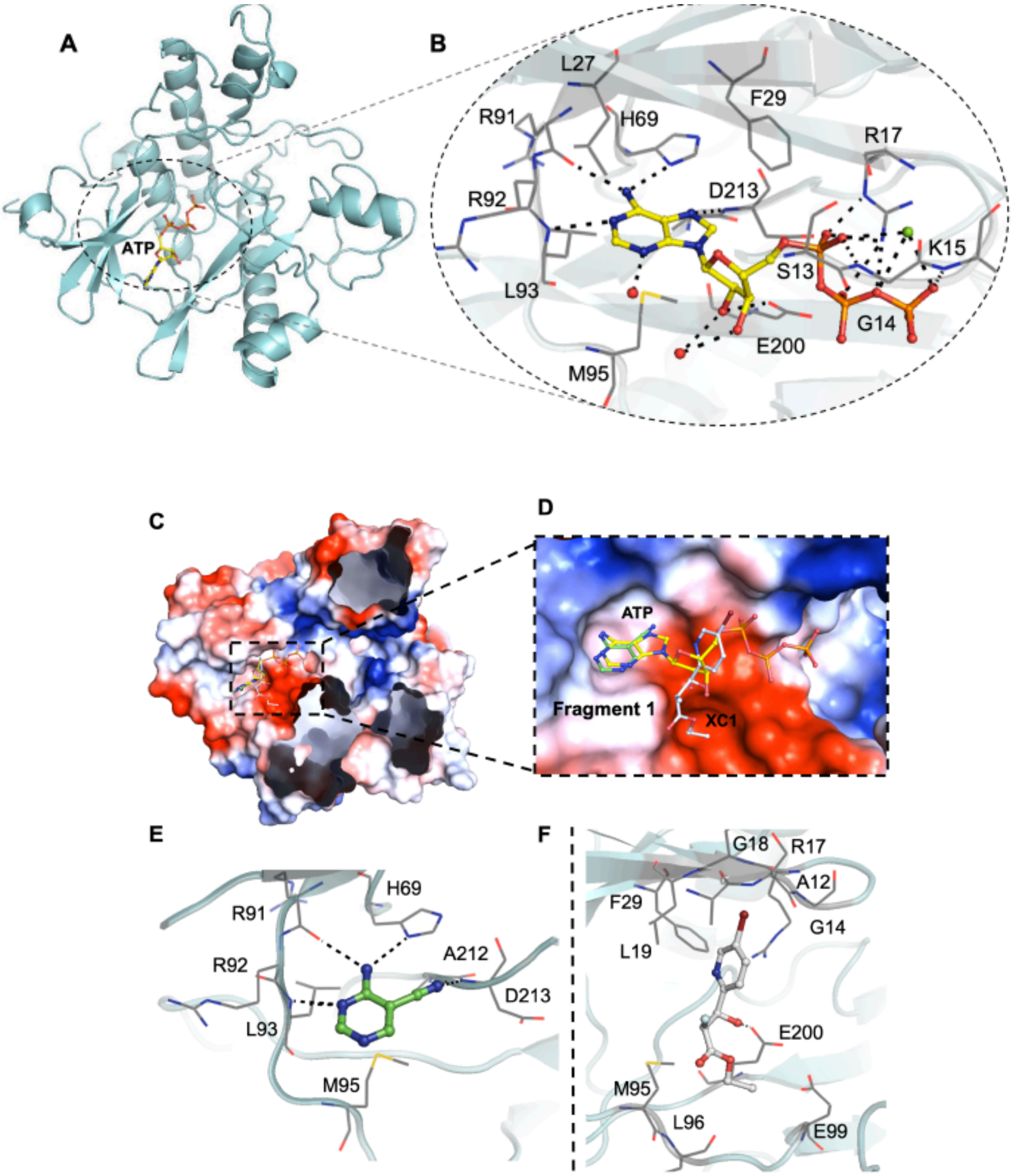

Figure 2. (a and b) X-ray crystal structure of *Mab* PurC in complex with ATP (PDB code 6YX3). ATP is shown in yellow stick model with the sidechain and key interactions within the active sites highlighted, water molecules as red and Mg^{2+} as green spheres respectively (c and d) Overlay of the fragment **1** (PDB code 6Z0R) and fragment **2** (PDB code 6Z0Q) in ATP bound PurC (e) Interactions of fragment **1**, shown in green stick model, with PurC. (f) Interactions of fragment **2**, shown as gray stick model, with PurC. The amino acids are represented as gray line model.

Prior to hit-to-lead elaboration, further DSF was performed on a number of close analogues of fragment **1** to examine preliminary SAR around the pyrimidine pharmacophore. As shown in Table 1, a comparison between fragment **1** (K_d = 341 μM, LE 0.53) and compound **4** (K_d = 1060 μM, LE 0.45) shows that the pyrimidine analogue exhibits a higher ΔT_m and a 3-fold increase in the binding affinity compared to pyridine counterparts. The addition of a chlorine atom at the 6-position of the pyrimidine ring is tolerated as shown in compound **3** (K_d = 159 μM, LE 0.52) when compared to the original fragment **1**. The replacement of a nitrile with a chlorine atom (compounds **3** vs **6**) decreases ΔT_m and shows a slight decrease in binding affinity (for compound **6**; K_d = 442 μM, LE 0.51). This substitution could be beneficial for fine-tuning the physicochemical properties of lead compound later in the optimisation as compounds with a chlorine substituent show a higher clogP and lower PSA compared to compounds with a nitrile functional group.[31] However, the removal of H-bond acceptor at this position (CN or Cl) diminishes the change in the melt-temperature (ΔT_m) completely as seen in compound **8**. This shows the significance of having H-bonding acceptor present at the 5-position of pyrimidine. The change to the ring to a pyrazine ring **5** and the removal of N1 in pyrimidine **4** and **7** and removal of the cyano-group in the 5-position **8**, all had a detrimental effect on the ΔT_m.

Table 1: Biophysical data for selected fragments showing the change in protein melting temperatures (ΔT_m), binding affinities (K_d) and ligand efficiencies (LE).

Compound	Chemical structure	ΔT_m (°C)[a]	*Mab*PurC K_d (μM)	LE[c]
1	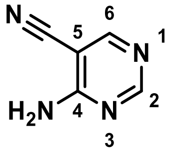	+3.6	341 ± 14	0.53
2	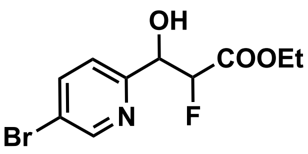	ND	ND	-

3	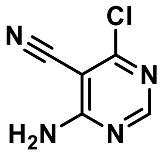	+4.0	159 ± 9	0.52
4	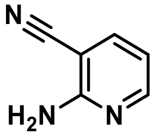	+1.7[b]	1060 ± 252	0.45
5	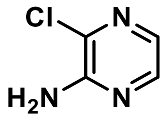	+1.0	971 ± 29	0.51
6	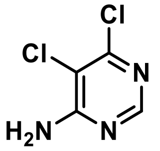	+2.5	442 ± 22	0.51
7	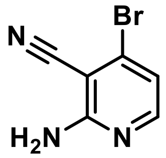	+1.7	ND	-
8	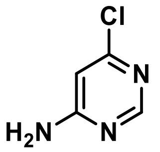	+0.7	ND	-

[a] 5 mM ligand and 100 μM *Mab*PurC

[b] 3 mM ligand and 70 μM *Mab*PurC

[c] kcal mol^{-1} per heavy atom

ND not determined

Hit-to-Lead optimisation

Fragment **1** was selected for further elaboration due to it having the highest ligand efficiency (LE) in the series. A closer examination of the X-ray crystal structure of fragment **1** with *Mab* PurC reveals a vector for elaboration, into the ‘ribose binding pocket’, at the 6-postion of the pyrimidine, which could be explored as an area for fragment growth as it is tolerated as seen in compound **3**. Utilising fragment elaboration at this position would allow the possibility of adding the feature of the pyridine moiety of fragment **2** into fragment **1**. These two fragments are almost perpendicular to each other and therefore it is necessary that a flexible linker be identified to join them together.

As shown in Table 2, the addition of a 4-pyrazolyl moiety effectively enhanced the binding affinity by an order of magnitude resulting in the identification of compound **9** (K_d = 23 μM, LE 0.39). Even though the X-ray crystal structure of *Mab*PurC in complex with compound **9** shows that the pyrazole does not make any significant polar interactions to *Mab*PurC as demonstrated in Figure 3b, all the original polar contacts of the pyrimidine core have been retained. It is worth noting that the attached pyrazole **9** or pyridine (compounds **10** and **11**) and the pyrimidine core align in a coplanar fashion (Figure 3).

Table 2: Exploration of SAR on the 6-position of the pyrimidine ring against *Mab*PurC

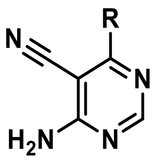

Compound	R	ΔT_m (°C)[a]	*Mab*PurC K_d (μM)	LE[b]
1	H	+1.1	341 ± 14	0.53
3	Cl	+2.1	159 ± 9	0.52
9	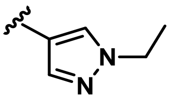	+4.4	23 ± 3	0.39
10	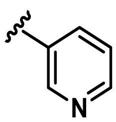	+2.0	588 ± 26	0.28
11	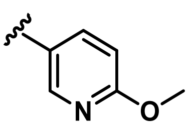	+2.6	84 ± 10	0.33

[a] 1 mM ligand and 100 μM *Mab* PurC

[b] kcal mol^{-1} per heavy atom

Following the identification of compound **9**, guided by the structural information, various flexible groups and saturated side chains were examined in order to identify the best substituent to incorporate (Table 3). The morpholine ring was employed in a number of analogues **12**, **13** and **15** to assist with the solubility of the compounds. The compound **14** (K_d = 22 μM, LE 0.32) which has an ethyl ester side chain was chosen and, although an increase in its binding affinity was not observed, the added hydrophobic ethyl ester was identified by X-ray crystallography close to the region where the pyridine moiety of fragment **2** is located, Figure 3d. A similar binding mode was also observed in the X-ray crystal structure of **13** (K_d = 52 μM, LE 0.26), Figure 3c. Interestingly, the ethyl morpholine group in **13** occupies almost the same site as the pyridine in fragment **2**. Even though these two compounds (**14** and **13**) did not show further improvement in binding affinity to *Mab*PurC, the corresponding X-ray crystal structures have provided the critical information necessary for further fragment optimisation (Figure 3c and d).

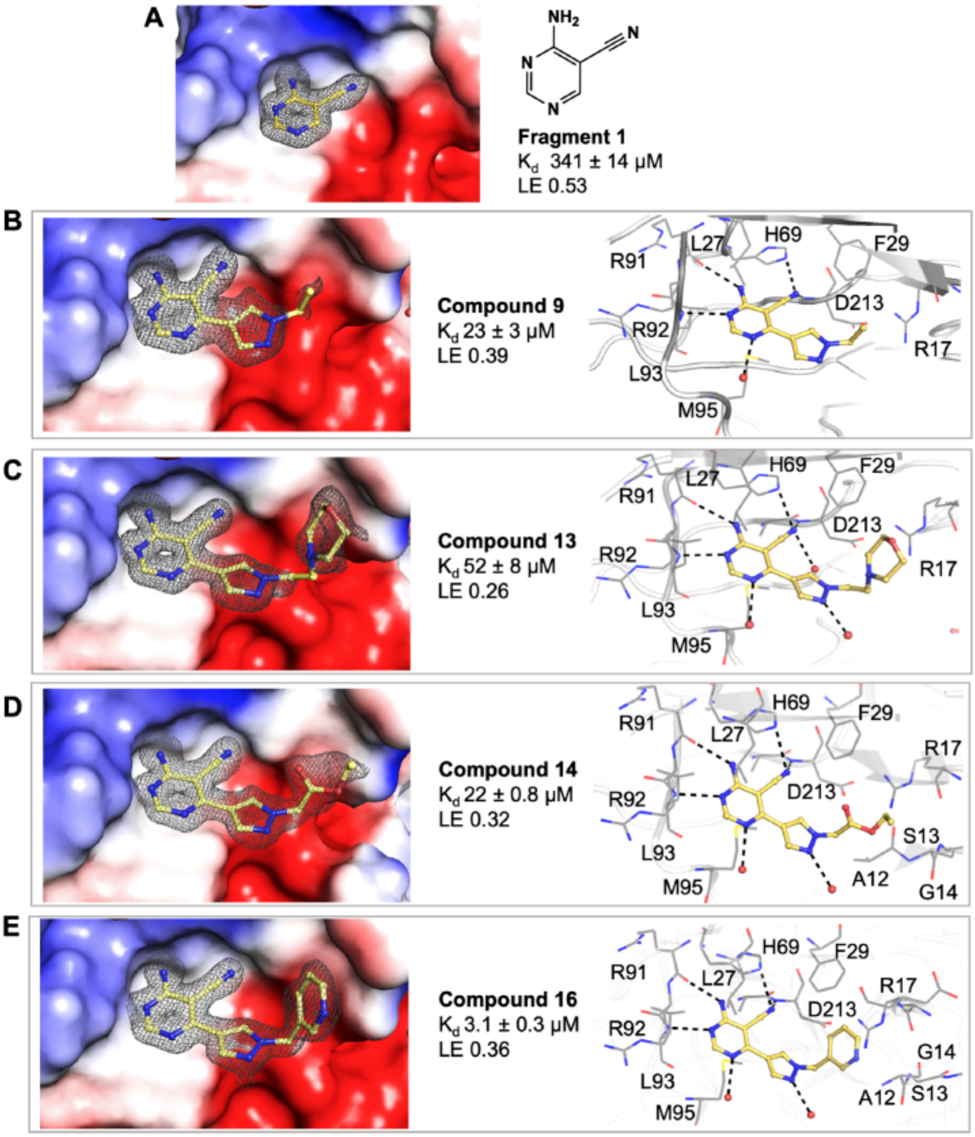

Figure 3. (a) Surface electrostatic representation of the X-ray crystal structures of Mab PurC in complex with fragment **1** (PDB code 6Z0R), occupying the ATP adenine pocket (b-e) *Mab* PurC in complex with compound **9** (PDB code 6YY6), **13** (PDB code 6YY8), **14** (PDB code 6YY7) and **16** (PDB code 6YY9) with the corresponding side chain and key interactions within the active sites illustrated beside each figure. The ligands are shown as yellow stick model with the respective electron density map (|Fo|−|Fc| omit map) contoured at 2.0σ presented in gray mesh. The interacting amino acids are shown in gray line representation.

Based on the X-ray crystal structure of *Mab*PurC in complex with compound **13**, it was proposed that the incorporation of 3-pyridylmethyl moiety at the N1 of the pyrazole ring would mimic the compound characteristics that engage the π-interaction seen with the pyridine moiety of fragment **2**. The resulting compound **16** (K_d = 3.1 μM, LE 0.36) shows an order of magnitude increase in its binding affinity compared to compound **13**. The alignment of this pyridine ring of compound **16** in the *Mab*PurC binding site by forming π-stacking interaction to R17 side chain is crucial for the enhanced affinity observed (Figure 3e, Table 3).

Table 3: Biophysical data of 4-amino-6-(pyrazol-4-yl)pyrimidine derivatives against *Mab*PurC

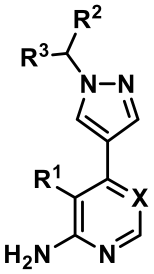

Compound	R1	R2	R3	X	ΔT_m (°C)[a]	*Mab*PurC K_d (μM)	LE[c]
9	CN	Me	H	N	+4.4	23 ± 3	0.39
12	CN	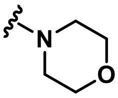	=O	N	+2.9	45 ± 5	0.27
13	CN	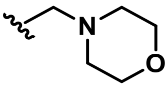	H	N	+3.5	52 ± 8	0.26
14	CN	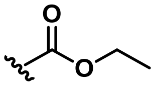	H	N	+4.5	22 ± 0.8	0.32
15	CN	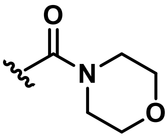	H	N	+2.6	47 ± 6	0.26
16	CN	3-pyridyl	H	N	+6.2	3.1 ± 0.3	0.36
17	CN	4-pyridyl	H	N	+6.0	7.5 ± 0.5	0.33
18	CN	5-methoxy-3-pyridyl	H	N	+6.5	2.1 ± 0.2	0.34
19	CN	3-fluorophenyl	H	N	+8.3	0.25 ± 0.03	0.41
20	CN	3-(trifluoromethyl)phenyl	H	N	+5.3	ND	-

21	CN	3-fluoro-5-methoxyphenyl	H	N	+8.8[b]	ND[d]	-
22	CN	4-fluorophenyl	H	N	+9.4	0.22 ± 0.02	0.41
23	CN	phenyl	H	N	+9.3	0.28 ± 0.03	0.43
24	CN	phenyl	Me	N	+7.5	0.53 ± 0.03	0.38
25	CN	benzyl	H	N	+5.3	ND	-
26	CN	3,5-difluorophenyl	H	N	+8.7[b]	0.24 ± 0.05	0.37
27	CN	3,4-difluorophenyl	H	N	+9.0	0.15 ± 0.02	0.37
28	Cl	3-fluorophenyl	H	N	+7.1	0.35 ± 0.02	0.39
29	CN	3-fluorophenyl	H	CH	+5.1	1.4 ± 0.06	0.36
30	Cl	3-fluorophenyl	H	CH	+2.6[b]	ND	-
31	H	3-fluorophenyl	H	N	+4.1	ND	-

[a] 1 mM ligand and 100 μM *Mab* PurC

[b] 0.5 mM ligand and 100 μM *Mab* PurC

[c] kcal mol^{-1} per heavy atom

[d] due to poor solubility

ND not determined

Various substituted phenyl and pyridyl rings were examined to investigate the effect of the aromatic rings in forming the π interaction to R17. It is generally accepted that fluorobenzene is a good isostere of pyridine due to the similarity in dipole and electron density.[32] There are many successful examples of an aryl C-F mimicking an azine nitrogen atom in drug discovery.[33] This change is also deemed as a way to modulate the physicochemical properties of the compound as removing a nitrogen atom will reduce the compound's basicity and increase its clogP at the same time. A number of analogues were synthesized including pyridylmethyl and fluorobenzyl side chains. Compound **19** (K_d = 0.25 μM, LE 0.41) featuring 3-flurophenyl moiety shows another order of magnitude improvement in binding affinity while all key interactions to *Mab*PurC are still observed in the corresponding X-ray crystal structure, Figure 4a.

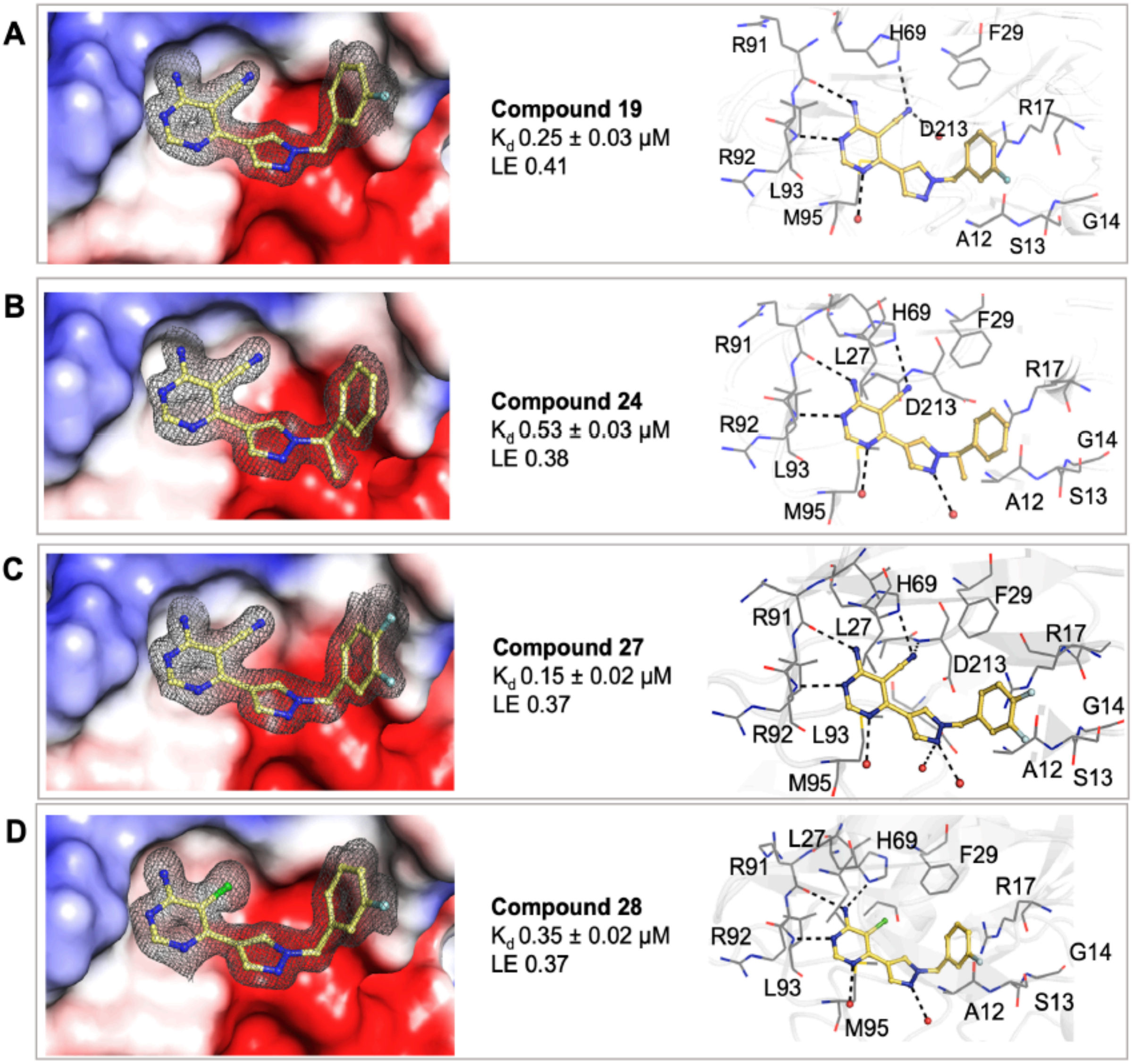

Figure 4. Surface electrostatic representation of the X-ray crystal structures of *Mab* PurC in complex with (a) compound **19** (PDB Code 6YYA), (b) compound **24** (PDB Code 6YYB), (c) compound **27** (PDB Code 6YYD) and (d) compound **28** (PDB code 6YYC) with the side chain and key interactions within the active sites illustrated beside each figure. The ligands are shown as yellow stick model with the respective electron density map (|Fo|−|Fc| omit map) contoured at 2.0σ presented in gray mesh. The interacting amino acids are shown in gray line representation.

The modulation of the electronic nature of this aryl ring in compound **19** is crucial to the affinity jump observed and various substituted phenyl analogues with electron-withdrawing and electron-donating groups were subsequently synthesized to test this hypothesis. The fluorine substituted compounds **22** (K_d = 0.22 μM, LE 0.41) and **27** (K_d = 0.15 μM, LE 0.37), Figure 4c, retain a strong binding affinity as observed in compound **19**. Interestingly, compound **23** possessing an unsubstituted phenyl ring also gave a K_d = 0.28 µM, LE 0.43. Compound **24** (K_d = 0.53 µM, LE 0.38) where a methyl group was introduced on the methylene carbon, a derivative of compound **23**, also displays a good affinity suggesting that this modification is tolerated this could possibly offer a further vector for elaboration, Figure 4b.

The fragment SAR (Table 1) had shown that the interchange between the CN and Cl moieties is tolerated and the removal of the N1 atom in pyrimidine has a dramatic negative effect on binding affinity. As shown in Table 3, each compound (**28**, **29**, **30**, and **31**) shares the same 3-fluorophenyl side chain as **19** but with a slightly different core structure. Compound **28** (K_d = 0.35 µM, LE 0.39) possessing a chlorine atom at the 5-position of pyrimidine rather than a nitrile group, exhibits a similar binding affinity as compared to **19**, Figure 14d, whereas compounds **29** and **30** led to a decrease in binding affinities. This observation corresponds to the results observed in early fragment SARs and could be important for further optimisation, as the derivatives containing a Cl substituent would possess a higher lipophilicity in comparison to compounds having a CN moiety and therefore could play additional roles in determining compound permeability and retention in the mycobacteria

Phenotypic screening of compounds against Mab and Mtb

The minimal inhibitory concentrations (MIC) of the selected compounds with K_d < 50 µM were determined for both *M. abscessus* and *M. tuberculosis in vitro* (Table 4). The compounds were screened against *Mtb* as there is an overall percentage identity between the *Mab* and *Mtb* PurC orthologues of 75%. The important active site residues and those involved in the interactions with the compounds described above are 100% conserved between *Mab* and *Mtb* PurC (see Figure S7). Almost all the compounds elaborated from the fragments exhibited complete growth inhibition at 50-200 µM against *Mab.* Whereas the compounds exhibited growth inhibition of 50 µM against *Mtb*, compounds **28** and **29** showed more promising inhibitory activity at 25 µM against *Mtb* (Table 3). The lack of significant MIC against *Mab* and *Mtb* show the challenges of developing small molecules against mycobacteria. This lack of activity could be due to a number of factors. For example *Mab* has been shown to have a large number of efflux pumps and any small molecules which get across the cell wall could be effluxed back out through these. In order to understand whether the compounds were getting across the *Mab* cell wall and engaging with PurC hypoxanthine rescue experiments were carried out. Hypoxanthine can be used as a salvage pathway of purine biosynthesis where this is converted to inosine monophosphate (IMP) by hypoxanthine-guanine phosphoribosylreansferase (HGPRT) (Scheme 1). Compound **19** was examined with varying concentrations of hypoxanthine (Figure S8) however the results were inconclusive. While there seems to be rescue at a concentration of 200 μM, this is at the limit of the MIC measured. The chemotypes which have been identified that get into *Mab* tend to vary significantly. Many of the current antibiotics used to treat *Mab* infections have LogP less than zero (for example the aminoglycoside Amikacin) and many of these are highly hydrophilic. However, small molecule inhibitors (for example those targeting Mmpl3 from *Mab*) which have been developed and show measurable effects on mycobacteria tend to have a LogP > 4.[34] The compounds that were developed in this work have LogP values which range from -1.6 to 2.2, which could possibly explain the lack of activity on *Mab*.

Further work is currently ongoing firstly to further optimise the compounds developed and secondly to understand how these compounds engage with PurC within *Mab*.

Table 4: Antimycobacterial profile of 4-amino-6-(pyrazol-4-yl)pyrimidine derivatives screened against *Mab* and *Mtb*

Compound	*Mab* PurC K_d (μM)	LogP[a]	*Mab* MIC (μM)[b]	*Mtb* MIC (μM)[c]
Amikacin	NA	-8.9	3.1	12.5
12	45 ± 5	-0.8	50-200	NA
13	52 ± 8	-0.6	50-200	NA
14	22 ± 0.8	-0.4	50-200	NA

15	47 ± 6	-1.6	200-400	50
16	3.1 ± 0.3	0.2	50-200	50
17	7.5 ± 0.5	0.2	50-200	50
18	2.1 ± 0.2	0.03	50-200	50
19	0.25 ± 0.03	1.6	50-200	50
22	0.22 ± 0.02	1.6	50-200	50
23	0.28 ± 0.03	1.5	50-200	50
24	0.53 ± 0.03	1.8	50-200	50
26	0.24 ± 0.05	1.8	50-200	50
27	0.15 ± 0.02	1.8	50-200	50
28	0.35 ± 0.02	2.2	50-200	25
29	1.4 ± 0.06	1.8	50-200	25

a) LogP was calculated using ChemDraw™ Professional Version 20.0
b) *Mycobacterium abscessus subspecies abscessus* (ATCC 19977) transformed with pmv310 plasmid expressing Lux ABDCE operon, grown in Middlebrook 7H9 broth supplemented with ADC
c) *Mycobacterium tuberculosis* ΔleuD ΔpanCD (Bleupan) transformed with pSMT1 expressing Lux AB and GFP, grown in Middlebrook 7H9 broth supplemented with 0.5% glycerol, 0.05% Tween 80 (removed for 24 h prior to experiments), 10% OADC (BD), 0.05 mg/mL L-leucine, and 0.024 mg/mL calcium pantothenate, Hygromycin and Zeocin (removed for 24 h prior to experiments).

Synthetic Chemistry

The early compounds in the series were synthesized following the routes shown in Scheme 2. Compounds **9**, **10** and **11** were synthesized using a Suzuki coupling reaction between pyrazole boronic acid **32** or pyridine boronic acids **33** and **34** and 4-amino-6-chloropyrimidine-5-carbonitrile **3** using $Pd(t\text{-}Bu_3P)_2$ as a catalyst in the presence of KF to afford the desire products. These were obtained in moderate to good yields (69 % yield for **9**, 25 % for **10** and 24 % for **11**).[35] Compound **12** was synthesized from its corresponding 4-iodopyrazole **35** and 4-morpholinecarbonyl chloride to afford compound **36**. This then underwent a Miyaura borylation reaction using B_2pin_2 in the presence of $Pd(dppf)Cl_2$ catalyst to yield the boronate ester **37** in good yield (53%).[36] The boronate ester **37** was then reacted with the 4-amino-6-chloropyrimidine-5-carbonitrile **3** heterocycle using Suzuki reaction conditions ($Pd(t\text{-}Bu_3P)_2$, KF, under MW irradiation, 150 °C over 40 minutes) to obtain **12** in 37% yield. Compounds **13**, **14** and **15** were synthesized from the corresponding pyrazole boronate esters and 4-amino-6-chloropyrimidine-5-carbonitrile under the Suzuki reaction conditions to yield the products in moderate yields (32% yield for **13**, 38% for **14** and 19% for **15**).[36]

Scheme 2. Synthesis of 4-aminopyrimidine and 2-aminopyridine derivatives

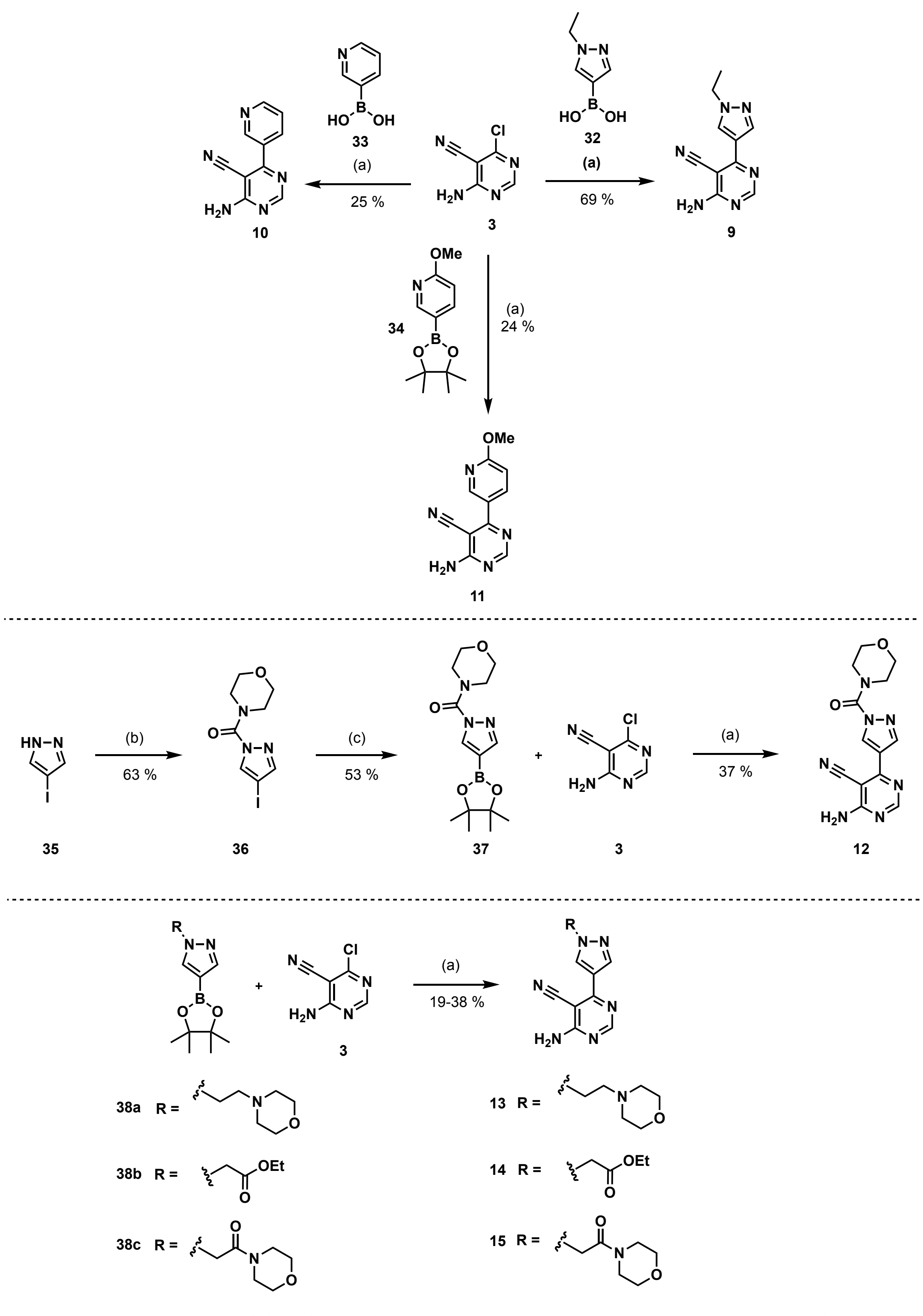

Reagents and Conditions: (a) Pd(t-Bu$_3$P)$_2$, KF, 1,4-dioxane, water, MW irradiation, 150 °C, 40 min; (b) 4-morpholinecarbonyl chloride, Et$_3$N, DCM, overnight; (c) B$_2$pin$_2$, Pd(dppf)Cl$_2$.DCM, KOAc, DMSO, MW irradiation, 80 °C, 3 h.

For most of the final products in the series (**16-31**), as depicted in Scheme 3, the synthesis began with the substitution reaction between pyrazole-4-boronic acid pinacol ester and an alkyl halide of choice (**39-50**) in the presence of a carbonate base (Cs_2CO_3 or K_2CO_3) to obtain the corresponding N-alkylated pyrazole boronate esters (**51-62**) in moderate to good yields (31% to quantitative yield).[37] The Suzuki coupling reactions under the same conditions as described previously using $Pd(t\text{-}Bu_3P)_2$ as a catalyst, was employed in the preparation of the final compounds resulting in 20-81% yield of the desired products.

Compound **7** was prepared according to the reported literature procedure starting from the bromination reaction of 4-methoxy-2-pyridone using phosphorus oxybromide ($POBr_3$) followed by nucleophilic amination using aqueous ammonia to replace the bromine at the 2-position of pyridine.[38] Compound **29** was synthesized using the same conditions as that for the Suzuki coupling reaction between previously prepared compound **54** and compound **7** in 61% yield. The synthesis of **30** began with the Suzuki coupling reaction between **54** and 2,3-dichloro-4-iodopyridine **65**. The reaction proceeded in a 56% yield of **66** with 4-iodo moiety being replaced with a pyrazole side chain. Compound **66** underwent a palladium-catalysed Buchwald-Hartwig reaction with benzophenone imine and the imine product obtained was then hydrolysed *in situ* under an acidic conditions using 1M HCl to afford the desired 2-aminopyridine **30** (63% yields over 2 steps).[39]

Scheme 3. Synthesis of 4-aminopyrimidine and 2-aminopyridine derivatives

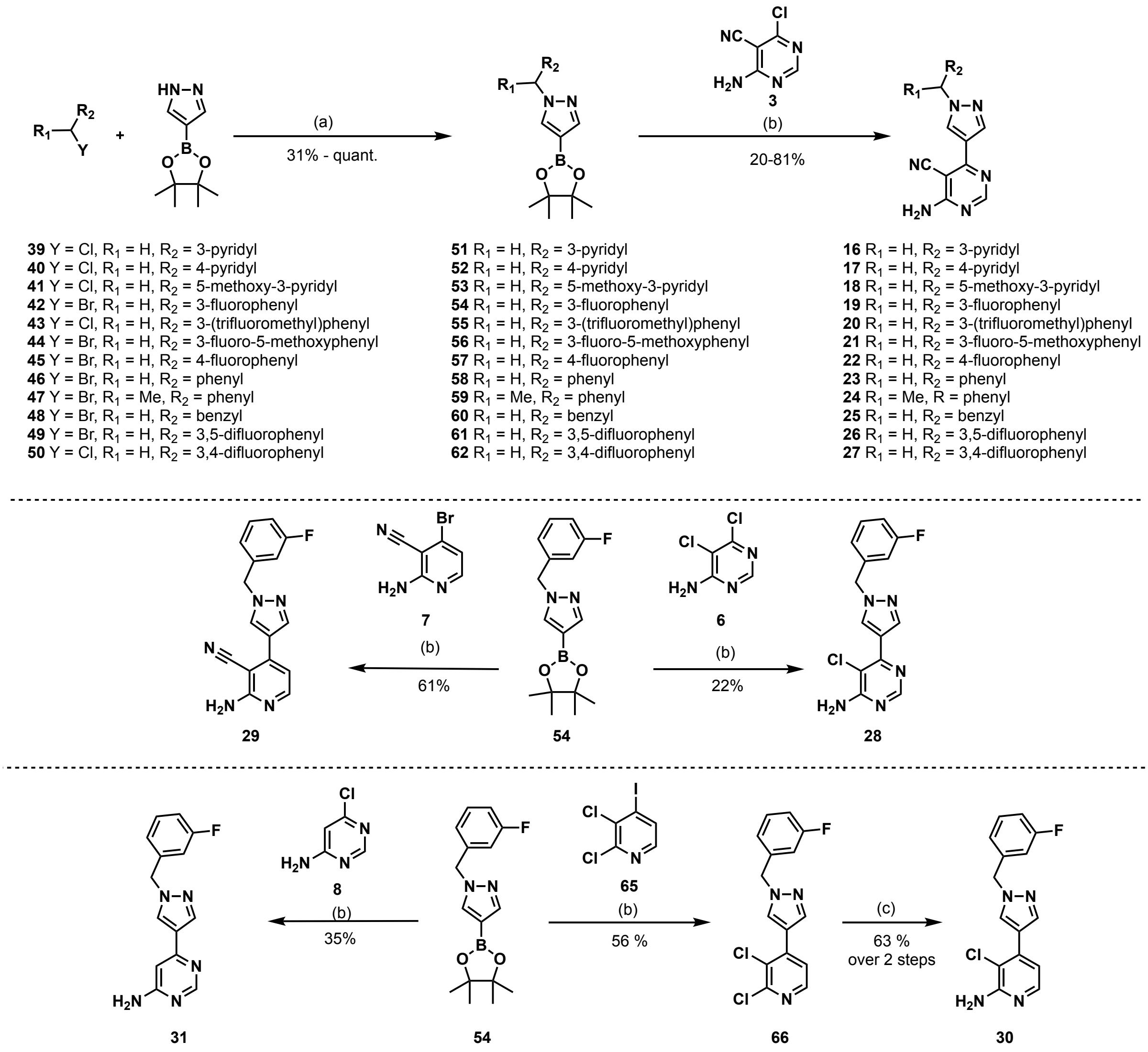

39 Y = Cl, R_1 = H, R_2 = 3-pyridyl
40 Y = Cl, R_1 = H, R_2 = 4-pyridyl
41 Y = Cl, R_1 = H, R_2 = 5-methoxy-3-pyridyl
42 Y = Br, R_1 = H, R_2 = 3-fluorophenyl
43 Y = Cl, R_1 = H, R_2 = 3-(trifluoromethyl)phenyl
44 Y = Br, R_1 = H, R_2 = 3-fluoro-5-methoxyphenyl
45 Y = Br, R_1 = H, R_2 = 4-fluorophenyl
46 Y = Br, R_1 = H, R_2 = phenyl
47 Y = Br, R_1 = Me, R_2 = phenyl
48 Y = Br, R_1 = H, R_2 = benzyl
49 Y = Br, R_1 = H, R_2 = 3,5-difluorophenyl
50 Y = Cl, R_1 = H, R_2 = 3,4-difluorophenyl

51 R_1 = H, R_2 = 3-pyridyl
52 R_1 = H, R_2 = 4-pyridyl
53 R_1 = H, R_2 = 5-methoxy-3-pyridyl
54 R_1 = H, R_2 = 3-fluorophenyl
55 R_1 = H, R_2 = 3-(trifluoromethyl)phenyl
56 R_1 = H, R_2 = 3-fluoro-5-methoxyphenyl
57 R_1 = H, R_2 = 4-fluorophenyl
58 R_1 = H, R_2 = phenyl
59 R_1 = Me, R_2 = phenyl
60 R_1 = H, R_2 = benzyl
61 R_1 = H, R_2 = 3,5-difluorophenyl
62 R_1 = H, R_2 = 3,4-difluorophenyl

16 R_1 = H, R_2 = 3-pyridyl
17 R_1 = H, R_2 = 4-pyridyl
18 R_1 = H, R_2 = 5-methoxy-3-pyridyl
19 R_1 = H, R_2 = 3-fluorophenyl
20 R_1 = H, R_2 = 3-(trifluoromethyl)phenyl
21 R_1 = H, R_2 = 3-fluoro-5-methoxyphenyl
22 R_1 = H, R_2 = 4-fluorophenyl
23 R_1 = H, R_2 = phenyl
24 R_1 = Me, R = phenyl
25 R_1 = H, R_2 = benzyl
26 R_1 = H, R_2 = 3,5-difluorophenyl
27 R_1 = H, R_2 = 3,4-difluorophenyl

Reagents and Conditions: (a) K_2CO_3 or Cs_2CO_3, MeCN, overnight; (b) Pd(*t*-Bu_3P)$_2$, KF, 1,4-dioxane, water, MW irradiation, 150 °C, 40 min; (c) (i) $Pd_2(dba)_3$, BINAP, *t*-BuONa, benzophenone imine, toluene, 80 °C, overnight (ii) 1 M HCl, THF, 5 h.

CONCLUSION

The application of a fragment-based approach towards the discovery of novel inhibitors of *M. abscessus* PurC is described. A combination of in-house fragment screening and high-throughput X-ray crystallographic screening provided crucial starting points for the fragment elaboration process. The fragment growing and merging strategies combined the structural characteristics of the two parent fragments, fragment **1** and fragment **2**. The hit-to-lead elaboration, guided by X-ray crystallographic information and binding affinity data, resulted in the identification of compound **19** (K_d 250 nM, LE 0.41) and compound **27** (K_d 150 nM , LE 0.39) both possessing promising *in vitro* binding affinities. The fragment growing and merging approaches described further demonstrate the strength of fragment-based design in accelerating the overall hit-to-lead progression. These results are encouraging and this study, as a first example of designing inhibitors against bacterial PurC, shows the potential for developing novel antimicrobials targeting this enzyme. However this study also highlights the challenges in developing small molecules against targets in *M. abscessus*. While small molecules with high affinities can be developed using the fragment-based approach, the challenge is ensuring that these inhibitors get across the cell wall of *M. abscessus* and engage with the target *in vivo*. Work is currently underway to improve the overall physico-chemical profiles of the lead compounds described herein in order to enhance their affinity against *M. abscessus*.

METHODS

The charachterisation data for all the compounds described can be found in the supporting information.

Mycobacterium abscessus purC **gene knock-out studies**

Deletion of *purC* gene from *M. a. massiliense* CIP108297 was carried out by recombineering as described previously**.** Briefly, primers were designed to amplify 1000 bp flanking regions upstream and downstream of the gene. A streptomycin cassette obtained from pHP45W was cloned between these fragments to create an allelic exchange substrate (AES). *M. a. massiliense* containing a modified version of pJV53 with the *xylE* gene (pJV53-xylE) was induced for 4h with 0.2% acetamide and electroporated with 500ng of AES. Cells were incubated at 37C overnight and plated on 7H11 ADC containing Streptomycin 200 mg/mL for selection and hypoxanthine 20 mg/mL to complement growth of the mutant. After 5 days colonies were picked on plates with or without hypoxanthine and checked by PCR to confirm deletion of the gene.

Amplification of *purC* gene from *Mycobacterium abscessus* genomic DNA

Genomic DNA sample was obtained from *Mycobacterium abscessus* (ATCC 19977). The stock of genomic DNA (6 ng/mL) was diluted using sterile water to make a working concentration of 0.6 ng/mL. The *purC* gene (MAB_0689) was amplified using the following primers (Sigma):

Forward Primer: 5'-ATTCCATGGTGCGTCCTTCGCTGTCCGATTAC-3'

Reverse Primer: 5'-TATCTCGAGTCACGCCGACGGGCCAATCC-3'

The following thermocycle program was used: stage 1 x 1 cycle: activation of polymerase at 95 ^{o}C for 2 min, stage 2 x 35 cycles: denaturation at 95 ^{o}C for 20 s, annealing at 70 ^{o}C for 20 s, extension at 70 ^{o}C for 45 s. This was followed by stage 3: final extension at 70 ^{o}C for 10 min.

Molecular Cloning

The purified PCR product and a PHAT2 *E. coli* expression vector containing Amp^{r} and non-cleavable N-terminal His-tag were then subjected to restriction digestion with Nco1 and XhoI restriction endonucleases (ThermoScientific). The ligation of digested insert and vector was performed using T4 DNA ligase (New England Biolabs), by incubation at room temperature for 10 min. The ligation product was transformed in to *E. coli* DH5a competent cells by heat-shock method and plated on LB agar-kanamycin plates and incubated at 37 °C. Single colonies were randomly picked on the following day and inoculated in LB media with kanamycin (30 mg/mL) and grown overnight at 37 °C. Plasmids from the resulting cultures were isolated and purified (ThermoScientific GeneJet Plasmid Miniprep Kit). The integrity of the clones was confirmed by sequencing (DNA Sequencing Facility, Department of Biochemistry, University of Cambridge, UK).

Expression and Purification of PurC protein

E. coli BL21 (DE3) strains containing N-His-PurC pHAT2 plasmids were grown overnight at 37°C in LB-media containing Ampicillin (100 µg/mL). This seed-stage culture was used to inoculate 6 shake flasks containing 1 L each of 2XYT media with Ampicillin (100 µg/mL) until optical density (A_{600nm}) reached 0.6. Expression of recombinant construct was induced by the addition of Isopropyl β-D-1-thiogalactopyranoside (IPTG) to a final concentration of 0.5 mM and further allowed to grow at 18 °C for 16 h. Cells were harvested by centrifugation at 4°C for 20 min at 5000 g and the pellet was re-suspended in buffer A (50 mM Tris-HCl pH 7.5, 350 mM NaCl, 20 mM Imidazole). 10 µg/mL DNaseI, 5 mM $MgCl_2$ and protease inhibitor cocktail tablets (New England Biolabs) were added to the cell suspension. The cells were lysed by sonication (Branson) and the lysate was clarified by centrifugation at 4°C for 40 min at 25,568 g. The clarified lysate was filtered using a 0.45 µm syringe filter and passed through a pre-equilibrated (with buffer A) 10 mL pre-packed Nickel-sepharose column (HiTrap IMAC FF, GE Healthcare). The column was washed with 5 column volumes of buffer A and the bound protein was eluted as 2 x 12 mL elutes using buffer B (50 mM Tris-HCl pH 7.5, 350 mM NaCl and 500 mM Imidazole). The protein was analyzed on a 15 % SDS-PAGE gel and elutes from HiTrap IMAC column containing the sample protein were pooled and subjected to dialysis against 2 L of buffer C (50 mM Tris-HCl pH 7.5, 350 mM NaCl) overnight at 4°C. After overnight dialysis the protein was concentrated using a 10 kDa centrifugal concentrator (Sartorius Stedim) and loaded onto a pre-equilibrated (with buffer D: 50 mM Tris-HCl pH 7.5, 150 mM NaCl) 120 mL Superdex200 16/600 column (GE Healthcare). 2 mL fractions were collected and analyzed on a 15 % SDS-PAGE gel, followed by MALDI-Mass fingerprinting. Fractions corresponding to pure PurC protein were pooled, concentrated to 26 mg/mL, flash frozen in liquid nitrogen and stored at -80°C.

Crystallization of *M. abscessus* PurC

Screening of commercial sparse matrix libraries for the identification of appropriate crystallization conditions for *M. abscessus* PurC protein was performed as described previously.[20] Drops containing 18 mg/mL of the protein in storage buffer (50 mM Tris-HCl pH 7.5, 150 mM NaCl) and reservoir were set up at drop ratios: 1:1 and 2:1 (of protein: reservoir respectively) using a Mosquito crystallization robot (TTP labtech), in 96-well sitting drop plates. The drops were equilibrated against 80 µL of the corresponding reservoir solution at 19 °C. The best diffracting crystals were observed in the crystal condition containing 0.2 M $LiSO_4$, 0.1 M Bis-Tris pH 5.5, 25 % PEG 3350.

Soaking of fragments and compounds on PurC native crystals

Crystals for soaking were grown at 19°C in 48-well sitting drop plates in a grid consisting of 0.2 M Lithium sulphate, 21-28 % PEG 3350, 0.1 M Bis-Tris pH 5.5–6.5, set up at drop rations 1:1 µL (of protein reservoir respectively). The crystals appeared in 3 – 5 days and were then moved into 24-well hanging drop plates to allow soaking in 4 µL drops containing the respective reservoir solutions and 10 mM fragments/compounds. The drops were then equilibrated against 800 µL of the respective reservoir solution for 16 h at 19°C in 24-well hanging drop plates.

Co-crystallization of PurC protein with ATP and lead compounds

For co-crystallization of PurC, 18 mg/mL of the protein was mixed with 2 - 5 mM final concentration of the ligand/compound and incubated for 2 h on ice. The crystallization drops were set up using the incubated samples at a protein to reservoir drop ratio of 0.3 µL: 0.3 µL, in 96-well (MRC2) sitting drop plates in 0.2 M Lithium sulphate, 21-28 % PEG 3350, 0.1 M Bis-Tris pH 5.5–6.5 condition. The drops were equilibrated against 70 µL of reservoir at 19°C.

X-ray Data Collection and processing

The crystals were flash-cooled in cryo-solution consisting of 25 % ethylene glycol in the corresponding reservoir. X-ray data sets were collected at the Diamond Light Source in the UK, using rotation method at wavelength of 0.979 Å, Omega start: 0°, Omega Oscillation:

0.15°, Total images: 2100-2400, Exposure time: 0.05-0.08 s and at the French National Synchrotron facility (Soleil), at wavelength of 0.979 Å, Omega start: 0°, Omega Oscillation: 1°, Total oscillation: 210° -240° and Exposure time: 0.5 s. The diffraction images were processed using AutoPROC[40], utilizing XDS[41] for indexing, integration and POINTLESS[42], AIMLESS[43] and TRUNCATE[44] programs from CCP4 Suite[45] for data reduction, scaling and calculation of structure factor amplitudes and intensity statistics. PurC ligand bound structures were solved by molecular replacement using PHASER[46] with the atomic coordinates of the *Mycobacterium abscessus* PurC apo structure as search model, as described previously.[20] Structures were refined using REFMAC[47] and PHENIX[48]. Model building was performed using COOT[49] interactive graphics program and electron density maps were calculated with 2|Fo|- |Fc| and |Fo| - |Fc| co-efficient. OMIT difference maps |mFo − DFc|[50] were calculated and analysed to verify positions of modelled ligands.

Thermal shift assay

Reactions were carried out in triplicate in a 96-well plate. Each reaction contained a final concentration of 20 µM PurC, 5x SYPRO Orange, 100 mM HEPES pH 7.5, 150 mM NaCl, 1 mM $MgCl_2$, 5 % DMSO and 5 mM for compounds **1-3** and **5-8**. Compound **4** was screened at a concentration of 3 mM and all other compounds were screened at a concentration of 1 mM. The plate was centrifuged briefly to remove bubbles and analysed in a Bio-Rad CFX96 Touch or CFX Connect RT-qPCR machine. Samples were incubated at 25 °C for 10 min and the temperature was then raised to 96 °C at a rate of 1 °C min^{-1} whilst fluorescence was recorded with excitation/emission wavelengths of 490/575 nm. Data were analysed in Microsoft Excel to calculate the melting temperature (T_m) and ΔT_m for each condition relative to the protein and DMSO-only control.

Isothermal titration calorimetry

ITC experiments were carried out in a buffer of 100 mM HEPES pH 7.5, 150 mM NaCl and 1 mM $MgCl_2$. Protein was dialysed against this buffer overnight before experiments and subsequent dilutions of protein and ligands used the remaining dialysis buffer. Generally, ligands at a concentration of 4 mM (ATP and CAIR), 2-5 mM (fragments and weakly-binding compounds) or 0.2-1.5 mM (strongly-binding compounds) were titrated against 20-100 μM PurC in a Malvern MicroCal iTC200 machine. To correct for enthalpy of dilution, ligands were also titrated against buffer and the peak values of this run subtracted from the experimental run as a reference. When ligands were dissolved in DMSO an appropriate concentration of DMSO (5-10 % v/v) was added to other solutions. Data were analysed using the Origin software (OriginLab, Northampton, MA, USA). The titration of an initial injection (0.2 μL) was discarded during data processing.

Phenotypic screening against *Mab*

M. abscessus subspecies *abscessus* (ATCC19977) was transformed with pmv310 plasmid expressing Lux ABDCE operon, grown in Middlebrook 7H9 broth supplemented with ADC (Sigma, UK). Minimum Inhibitory Concentrations (MIC) were determined according to the Clinical and Laboratory Standards Institute (CLSI) method M07-A9. *Mycobacteria* were grown to an OD600 of 0.2–0.3 (Jenway 6300 spectrophotometer) in liquid culture, and 1 × 10^5 bacteria were added to each well of 96-well plates containing serial dilutions of compound (400, 200, 100, 50, 25, 12.5, 6.3, 3.1, 1.6, 0.8, 0.4, 0 μM), in triplicate wells per condition, and incubated at 37 °C until growth was seen in the control wells. The MIC value was determined as the last well which showed no bacterial growth.

ASSOCIATED CONTENT

Supporting Information

The supporting information is available free of charge at https://pubs.acs.org/doi/xx.xxxx/acsinfecdis. Xxxxxxx

Compound synthesis and X-ray crystallography tables. LCMS of screened compounds.

ACKNOWLEDGMENTS

This paper is dedicated to the memory of Professor Chris Abell who passed away on the 26th October 2020. The authors would like to thank the Diamond Light Source for beam-time (proposals mx9537, mx14043, mx18548) and the staff of beamlines I03, I02, I04, I04-1 and I24 and the French National Synchrotron facility (Soleil) for assistance with data collection. The authors are grateful to Prof. Frank von Delft, Dr. Patrick Collins and the XChem team at the DLS I04-1 beamline for access to fragment libraries and the high-throughput fragment screening facility. We thank Prof. Adam Nelson and his group at the University of Leeds for the three-dimensional fragment library at the DLS XChem facility. SET was funded by the Cystic Fibrosis Trust and Fondation Botnar (Grant No. 6063). SC, SGG were funded by the Fondation Botnar (Grant No. 6063), AW was funded by the EPSRC. RAF is funded by the Cystic Fibrosis Trust Strategic Research Centre (SRC010) and Innovation Hub (IH01) awards, Wellcome Trust (I07032AIA) and Royal Papworth Hospital Research Award. VM was funded by the Bill and Melinda Gates Foundation SHORTEN-TB (OPP1158806). TLB is funded by the Wellcome Trust (Investigator Award 200814_Z_16_Z). MJ and JMB are funded by the Cystic Fibrosis Strategic Research Centre (SRC010), MAGdE is funded by the American Leprosy Mission (G88726).

Abbreviations

SAICAR- phosphoribosylaminoimidazole-succinocarboxamide; *Mab* - *Mycobacterium abscessus*; *Mtb* - *Mycobacterium tuberculosis*; DSF - differential scanning fluorimetry; ITC – isothermal titration calorimetry; SAR – structure activity relationship; PSA- polar surface area; LE – ligand efficiency.

Author Contributions

CA, AGC, TLB, RAF, VM and MJ designed and supervised the project. SC, AC, AJW, SGG synthesized the compounds used in this study. SET and MAGdE carried out the structural biology and biochemical studies. KB and JS devised and carried out the screening of the compounds against *Mab* and *Mtb*. JMB and MJ generated the knockout mutants. SC, SET and AGC wrote the manuscript and all authors commented on the final version of the manuscript.

REFERENCES

1. Liu, H., Dong, F., Liu, J., Liu, J., Pang, Y., Zhao, S., Lu, J., Li, H. (2019) Successful management of *Mycobacterium abscessus* complex lung disease in an otherwise healthy infant. *Infect Drug Resist, 12*, 1277-1283.

2. Esther Jr, C. R., Esserman, D. A., Gilligan, P., Kerr, A., Noone, P. G., (2010), Chronic *Mycobacterium abscessus* infection and lung function decline in cystic fibrosis. *J Cyst Fibros*, *9* (2), 117-23.

3. Bar-On, O., Mussaffi, H., Mei-Zahav, M., Prais, D., Steuer, G., Stafler, P., Hananya, S. Blau, H. (2015) Increasing nontuberculous mycobacteria infection in cystic fibrosis. *J Cyst Fibros, 14* (1), 53-62.

4. Qvist, T., Taylor-Robinson, D., Waldmann, E., Olesen, H. V., Hansen, C. R., Mathiesen, I. H., Hoiby, N., Katzenstein, T. L., Smyth, R. L., Diggle, P. J., Pressler, T., (2016) Comparing the harmful effects of nontuberculous mycobacteria and Gram negative bacteria on lung function in patients with cystic fibrosis. *J Cyst Fibros, 15*, 380-5.

5. Chen, J., Zhao, L., Mao, Y., Ye, M., Guo, Q., Zhang, Y., Xu, L., Zhang, Z., Li, B., Chu, H., (2019) Clinical Efficacy and Adverse Effects of Antibiotics Used to Treat *Mycobacterium abscessus* Pulmonary Disease. *Front Microbiol, 10*, 1977.

6. Sfeir, M., Walsh, M., Rosa, R., Aragon, L., Liu, S. Y. Cleary, T., Worley, M.; Frederick, C.; Abbo, L. M., (2018) *Mycobacterium abscessus* Complex Infections: A Retrospective Cohort Study. *Open Forum Infect Dis*, *5* (2), ofy022.

7. Raats, D., Lorent, N., Saegeman, V. Vos, R.; van Ingen, J.; Verleden, G.; Van Raemdonck, D.; Dupont, L., (2019) Successful lung transplantation for chronic *Mycobacterium abscessus* infection in advanced cystic fibrosis, a case series. *Transpl Infect Dis, 21* (2), e13046.

8. Osmani, M., Sotello, D., Alvarez, S., Odell, J. A., Thomas, M. (2018) *Mycobacterium abscessus* infections in lung transplant recipients: 15-year experience from a single institution. *Transpl Infect Dis.,* **20** (2), e12835.

9. Moffatt, B. A., Ashihara, H. (2002) Purine and pyrimidine nucleotide synthesis and metabolism. *Arabidopsis Book, 1,* e0018.

10. Manjunath, K., Jeyakanthan, J., Sekar, K., (2015) Catalytic pathway, substrate binding and stability in SAICAR synthetase: A structure and molecular dynamics study. *J Struct Biol, 191 (1)*, 22-31.

11. Tuntland, M. L., Fung, L. W. (2016) Substrate independent ATPase activity may complicate high throughput screening. *Anal Biochem, 510*, 18-20.

12. Samant, S., Lee, H., Ghassemi, M., Chen, J., Cook, J. L., Mankin, A. S., Neyfakh, A. A., (2008) Nucleotide biosynthesis is critical for growth of bacteria in human blood. *PLoS Pathog,* 4 (2), e37.

13. Vogel-Scheel, J., Alpert, C., Engst, W., Loh, G., Blaut, M. (2010) Requirement of purine and pyrimidine synthesis for colonization of the mouse intestine by Escherichia coli. *Appl Environ Microbiol, 76* (15), 5181-7.

14. Wang, N., Ozer, E. A., Mandel, M .J., Hauser, A. R., (2014) Genome-wide identification of *Acinetobacter baumannii* genes necessary for persistence in the lung. *MBio, 5 (3)*, e01163-14.

15. Ginder, N. D., Binkowski, D. J., Fromm, H. J., Honzatko, R. B., (2006) Nucleotide complexes of *Escherichia coli* phosphoribosylaminoimidazole succinocarboxamide synthetase. *J. Biol. Chem., 281 (30)*, 20680-8.

16. Levdikov, V. M., Barynin, V. V., Grebenko, A. I., Melik-Adamyan, W. R., Lamzin, V. S., Wilson, K.S., (1998) The structure of SAICAR synthase: an enzyme in the de novo pathway of purine nucleotide biosynthesis. *Structure, 6* (3), 363-76.

17. Wolf, N. M., Abad-Zapatero, C., Johnson, M. E, Fung, L. W., (2014) Structures of SAICAR synthetase (PurC) from *Streptococcus pneumoniae* with ADP, Mg^{2+}, AIR and Asp. *Acta crystallographica. Section D, Biological crystallography, 70* (Pt 3), 841-50.

18. Zhang, R., Skarina, T., Evdokimova, E., Edwards, A., Savchenko, A., Laskowski, R. , Cuff, M. E., Joachimiak, A., (2006) Structure of SAICAR synthase from *Thermotoga maritima* at 2.2 angstroms reveals an unusual covalent dimer. *Acta crystallographica. Section F, Structural biology and crystallization communications, 62* (Pt 4), 335-9.

19. Li, S.X., Tong, Y.P., Xie, X. C., Wang, Q. H., Zhou, H. N., Han, Y., Zhang, Z. Y., Gao, W., Li, S. G., Zhang, X .C., Bi, R .C., (2007) Octameric structure of the human bifunctional enzyme PAICS in purine biosynthesis. *J Mol Biol, 366* (5), 1603-14.

20. Thomas, S. E., Collins, P., James, R. H., Mendes, V., Charoensutthivarakul, S., Radoux, C., Abell, C., Coyne, A. G., Floto, R. A., von Delft, F., Blundell, T. L., (2019) Structure-

guided fragment-based drug discovery at the synchrotron: screening binding sites and correlations with hotspot mapping. *Philos Trans A Math Phys Eng Sci., 377* (2147), 20180422.

21. Ducati, R. G., Breda, A., Basso, L. A., Santos, D. S., (2011) Purine Salvage Pathway in *Mycobacterium tuberculosis*. *Curr Med Chem, 18* (9), 1258-75.

22. Wolf, N. M., Abad-Zapatero, C., Johnson, M. E., Fung, L. W. M., (2014) Structures of SAICAR synthetase (PurC) from *Streptococcus pneumoniae* with ADP, Mg^{2+}, AIR and Asp. *Acta Crystallographica Section D Biological Crystallography, 70* (3), 841-850.

23. Murray, C. W., Newell, D. R., Angibaud, P. (2019), A successful collaboration between academia, biotech and pharma led to discovery of erdafitinib, a selective FGFR inhibitor recently approved by the FDA. *MedChemComm, 10* (9), 1509-1511.

24. Mendes, V., Blundell, T. L., (2017) Targeting tuberculosis using structure-guided fragment-based drug design. *Drug Discovery Today,* **22** (3), 546-554.

25. Scott, D. E., Coyne, A. G., Hudson, S. A., Abell, C. (2012) Fragment-based approaches in drug discovery and chemical biology. *Biochemistry, 51* (25), 4990-5003.

26. Collins, P. M., Douangamath, A., Talon, R., Dias, A., Brandao-Neto, J., Krojer, T., von Delft, F. (2018) Achieving a good crystal system for crystallographic X-Ray fragment screening. *Methods Enzymol, 610*, 251-264.

27. Pearce, N.M., Krojer, T., Bradley, A. R., Collins, P., Nowak, R. P., Talon, R., Marsden, B. D., Kelm, S., Shi, J., Deane, C. M., von Delft, F. (2017) A multi-crystal method for extracting obscured crystallographic states from conventionally uninterpretable electron density. *Nat Commun 8*, 15123.

28. Krojer, T., Talon, R., Pearce, N., Collins, P., Douangamath, A., Brandao-Neto, J., Dias, A., Marsden, B., von Delft, F. (2017) The XChemExplorer graphical workflow tool for routine or large-scale protein-ligand structure determination. *Acta Crystallogr D Struct Biol., 73* (Pt 3), 267-278.

29. Aimon, A., Karageorgis, G., Masters, J., Dow, M., Craven, P. G. E., Ohsten, M., Willaume, A., Morgentin, R., Ruiz-Llamas, N., Lemoine, H., Kalliokoski, T., Eatherton, A. J., Foley, D. J., Marsden, S. P., Nelson, A. (2018) Realisation of small molecule libraries based on frameworks distantly related to natural products. *Org. Biomol. Chem., 16 (17)*, 3160-3167.

30. Foley, D. J., Craven, P. G. E., Collins, P. M., Doveston, R. G., Aimon, A., Talon, R., Churcher, I., von Delft, F., Marsden, S. P., Nelson, A. (2017) Synthesis and Demonstration of the Biological Relevance of sp(3)-rich Scaffolds Distantly Related to Natural Product Frameworks. *Chem. Eur. J., 23* (60), 15227-15232.

31. Jones, L. H., Summerhill, N. W., Swain, N. A., Mills, J. E. (2010) Aromatic chloride to nitrile transformation: medicinal and synthetic chemistry. *MedChemComm, 1* (5). 309-318

32. Meanwell, N. A. (2018) Fluorine and Fluorinated Motifs in the Design and Application of Bioisosteres for Drug Design. *J Med Chem., 61* (14), 5822-5880.

33. Gillis, E. P., Eastman, K. J., Hill, M. D., Donnelly, D. J., Meanwell, N. A., (2015) Applications of Fluorine in Medicinal Chemistry. *J Med Chem., 58* (21), 8315-8359.

34. Li, W., Yazidi, A., Pandya, A. N., Hegde, P., Tong, W., de Moura, V. C. N., North, E. J., Sygusch, J., Jackson, M. (2018) Mmpl3 as a Target for the Treatment of Drug Resistant Nontuberculosis Mycobacterial Infections. *Front. Microbiol.*, 9, article 1547.

35. Williamson, D. S., Smith, G. P., Acheson-Dossang, P., Bedford, S. T., Chell, V., Chen, I. J., Daechsel, J. C. A., Daniels, Z., David, L., Dokurno, P., Hentzer, M., Herzig, M. C., Hubbard, R. E., Moore, J. D., Murray, J. B., Newland, S., Ray, S. C., Shaw, T., Surgenor, A. E., Terry, L., Thirstrup, K., Wang, Y., Christensen, K. V. (2017) Design of Leucine-Rich Repeat Kinase 2 (LRRK2) Inhibitors Using a Crystallographic Surrogate Derived from Checkpoint Kinase 1 (CHK1). *J Med Chem.,* 60 (21), 8945-8962.

36. Katz, J. D., Jewell, J. P., Guerin, D. J., Lim, J., Dinsmore, C. J., Deshmukh, S. V., Pan, B-S, Marshall, C. G., Lu, W. Altman, M. D., Dahlberg, W. K., Davis, L., Falcone, D., Gabarda, A. E., Hang, G., Hatch, H., Holmes, R., Kunii, K., Lumb, K. J., Lutterbach, B., Mathvink, R., Nazef, N., Patel, S. B., Qu, X., Reilly, J. F., Rickert, K. W., Rosenstein, C., Soisson, S. M., Spencer, K. B., Szewczak, A. A., Walker, D., Wang, W., Young, J., Zeng, Q., (2011) Discovery of a 5H-Benzo[4,5]cyclohepta[1,2-b]pyridin-5-one (MK-2461) Inhibitor of c-Met Kinase for the Treatment of Cancer. *J Med Chem,* **54** (12), 4092-4108.

37. Westaway, S. M., Preston, A. G. S., Barker, M. D., Brown, F., Brown, J. A., Campbell, M., Chung, C.-W., Drewes, G., Eagle, R., Garton, N., Gordon, L., Haslam, C., Hayhow, T. G. Humphreys, P. G., Joberty, G., Katso, R., Kruidenier, L., Leveridge, M., Pemberton, M., Rioja, I., Seal, G. A., Shipley, T., Singh, O., Suckling, C. J., Taylor, J., Thomas, P., Wilson, D. M., Lee, K., Prinjha, R. K., (2016) Cell Penetrant Inhibitors of the KDM4 and KDM5 Families of Histone Lysine Demethylases. 2. Pyrido[3,4-d]pyrimidin-4(3H)-one Derivatives. *J Med Chem., 59 (4)*, 1370-1387.

38. Trabanco, A. A., Tresadern G., Macdonald G. J., Vega, J. A., de Lucas, A. I., Matesanz E., García, A., Linares, M. L., Alonso de Diego, S. A., Alonso, J. M., Oehlrich, D., Ahnaou, A. , Drinkenburg, W., Mackie, C., Andrés, J. I., Lavreysen H., Cid, J. M. (2012) Imidazo[1,2-a]pyridines: Orally Active Positive Allosteric Modulators of the Metabotropic Glutamate 2 Receptor. *J Med Chem., 55* (6), 2688-2701.

39. Herr, R. J., Cioffi, C .L., Berlin, M. L. (2004) Convenient Palladium-Catalyzed Preparation of Primary Anilines Using a Fluorous Benzophenone Imine Reagent. *Synlett, 5*, 0841-0845.

40. Vonrhein, C. , Flensburg, C., Keller, P., Sharff, A., Smart, O., Paciorek, W., Womack, T., Bricogne T., (2011) Data processing and analysis with the AutoPROC toolbox. *Acta crystallographica. Section D, Biological crystallography, 67* (Pt 4), 293-302.

41. Kabsch, W., (2010) XDS, *Acta crystallographica. Section D, Biological crystallography 66* (Pt 2), 125-132.

42. Evans, P.R., (2011) An introduction to data reduction: space-group determination, scaling and intensity statistics. *Acta crystallographica. Section D, Biological crystallography 67* (Pt 4), 282-292.

43. Evans, P.R., Murshudov, G.N. (2013) How good are my data and what is the resolution? *Acta crystallographica. Section D, Biological crystallography, 69* (Pt 7), 1204-1214.

44. French, S.W.K. Wilson, K., (1978) On the treatmet of negatice intensity observations. *Acta Cryst. A34,* 517-525.

45. Winn, M.D., Ballard, C.C., Cowtan K.D., Dodson, E.J., Emsley, P., Evans, P.R., Keegan, R.M., Krissinel, E.B., Leslie, A.G., McCoy, A., McNicholas, S.J., Murshudov, G.N., Pannu, N.S, Potterton, E.A., Powell, H.R., Read, R.J., Vagin, A., Wilson, K.S. (2011) Overview of the CCP4 suite and current developments, *Acta crystallographica. Section D, Biological crystallography, 67* (Pt 4), 235-242.

46. McCoy, A.J., Grosse-Kunstleve, R.W., Adams, P.D., Winn, M.D., Storoni, L.C., Read, R. J. (2007) Phaser Crystallographic Software, *J Appl Crystallogr 40* (Pt 4), 658-674.

47. Murshudov, G.N., Skubak, P., Lebedev, A.A., Pannu, N.S., Steiner, R.A., Nicholls, R. A.,. Winn, M.D., Long, F., Vagin, A.A. (2011), REFMAC5 for the refinement of macromolecular crystal structures, *Acta crystallographica. Section D, Biological crystallography*, *67* (Pt 4), 355-367.

48. Adams, P.D., Afonine, P.V., Bunkoczi, G., Chen, V.B., Davis, I.W., Echols, N., Headd, J.J., Hung, L.W., Kapral, G.J., Grosse-Kunstleve, R.W., McCoy, A.J., Moriarty, N.W., Oeffner, R., Read, R.J., Richardson, D.C., Richardson, J.S., Terwilliger, T.C., Zwart, P.H. (2010) PHENIX: a comprehensive Python-based system for macromolecular structure solution. *Acta crystallographica. Section D, Biological crystallography*, *66* (Pt 2), 213-221.

49. Emsley, P., Cowtan, K. (2004) Coot: model-building tools for molecular graphics. *Acta Crystallographica. Section D, Biological crystallography 60* (Pt 12 Pt 1), 2126-2132.

50. Hodel, A., Kim, S-H, Brünger, A.T. (1992), Model Bias in Macromolecular Crystal Structures. *Acta Cryst. A, 48,* 851-858.

For Table of Contents Use Only